A Novel Two-Phase Mode Switching Control Strategy for PMSM Position Servo Systems With Fast-Response and High-Precision

Shaobin Li, Yongxiang Xu, *Member, IEEE*, Wentao Zhang, and Jibin Zou, *Senior Member, IEEE*

***Abstract*—In this article, a novel mode switching control (MSC) strategy is proposed containing a fast-response phase and a high-precision settling phase to meet the requirement of high-quality point-to-point permanent magnet synchronous motor servo systems. In the fast-response stage, an adaptive trajectory planning method is developed to program the *q*-axis current profile online based on the reference for the motor to reach the neighborhood of the reference position in minimum time. The chattering in the conventional time-optimal control is overcome and the idea that skipping speed and position loop with preplanned *q*-axis current trajectory is first attempted. After switching, the high-precision settling stage that is responsible for improving the transient performance in terms of reducing the overshoot and settling time is built with the proposed robust composite nonlinear feedback (RCNF) control law. This RCNF method cancels the overall disturbance through an extended state observer. The switching condition for the proposed MSC controller is clarified. Afterward, the whole closed-loop system's stability is strictly proved. Experiments are then conducted based on different scenarios to prove the effectiveness and robustness of the proposed MSC method.**

***Index Terms*—Adaptive trajectory planning (ATP), mode switching control (MSC), permanent magnet synchronous motor (PMSM), robust composite nonlinear feedback (RCNF).**

NOMENCLATURE

θ	Rotor mechanical position.
ω	Mechanical angular velocity.
K_t	Torque coefficient.
J	Moment of inertia.
d	External lumped disturbances.
r_0	Position reference.
t_f	Time needed to reach reference position.
u	Control law.
i_q	q-axis current.
$u_{\max}$ ($i_{\max}$)	Maximum allowed control input (q-axis current).
$\omega_{\max}$	Maximum allowed motor angular velocity.
$a_{\max}(a_0)$	Maximum allowed (nominal) acceleration of rotor.
$j_{\max}$	Maximum allowed jerk.
t_1 to t_7	Seven switching instants in the current profile.
t'_1 to t'_7	Modified switching instants by adaptation.
γ	Target position error band for switching.
p	Number of pole pairs.
ψ_{f0}, ψ_f	Nominal and real flux linkage.
T_L	Load torque.
T_f	Motor Coulomb friction.
T_{cog}	Cogging torque.
Q	Number of stator slots.
B	Viscous damping factor.
$\bar{a}$	Estimated motor acceleration.
S_1, S_2	Positions covered by the speed profile.
S_{temp}	Overlap of S_1 and S_2.
S_{c2}, S_{c2}	Critical boundary for position reference.
Δt	Compensation term by adaptation.
z_1, z_2, z_3	Estimated value of state variables.
L_1, L_2, L_3	ESO gains.
ω_c	ESO bandwidth.

Manuscript received 30 March 2022; revised 9 July 2022; accepted 19 August 2022. Date of publication 23 August 2022; date of current version 10 October 2022. Recommended for publication by Associate Editor K. Akatsu. *(Corresponding author: Jibin Zou.)*

The authors are with the School of Electrical Engineering and Automation, Harbin Institute of Technology, Harbin 150001, China (e-mail: flyingshaobin@gmail.com; xuyx@hit.edu.cn; zhang_wentaohit@163.com; zoujibin@hit.edu.cn).

Color versions of one or more figures in this article are available at https://doi.org/10.1109/TPEL.2022.3200969.

Digital Object Identifier 10.1109/TPEL.2022.3200969

I. INTRODUCTION

HIGH quality permanent magnet synchronous motor (PMSM) servo systems are always pursuing faster response and higher precision in the position tracking performance and is drawing increasingly attention in high-end applications such as optical disk drive, robotics, and aerospace field [1], [2]. Hence, enormous advanced control methods have been developed for PMSM servo systems, for instance, adaptive control [3], internal model control [4], predictive control [5], and iterative learning control [6]. Nevertheless, there is still much work to do such as increasing tracking speed and precision as well as reducing the calculation burden. Up till now, the most commonly applied control structure is the traditional three closed-loop cascaded PI control scheme for general servo systems. The method is simple, reliable, and effective but cannot fulfill fast response and smooth settling simultaneously. That is, a faster tracking speed incurs a larger overshoot with the settling time prolonged and vice versa. On the other hand, the anti-disturbance ability of PI controller is not satisfactory [7]. Also, the system's bandwidth decays from the innermost current loop to the outer

speed and position loops, which slows down the tracking process once again.

To overcome the problems above, a natural thought is to use the well-known time-optimal control (TOC) [8], [9] which uses the maximum or minimum allowed control signal generated by the so-called switching curves to achieve tracking with time-optimality. However, the corresponding chattering problem as well as its high sensitivity to disturbances and model uncertainties greatly handicaps the real application of this TOC method [11].

Scholars have developed a near time-optimality controller which is called proximate time-optimal servomechanisms (PTOS) to replace TOC. First proposed by Workman in [13], this controller draws a lot of attention especially in the hard disk drive (HDD) field. Essentially, PTOS is a mode switching control (MSC) strategy comprising three regions in the phase plane: an acceleration region where the maximum control signal is applied, an unsaturated area where the control is unsaturated, and a linear zone where the linear feedback control law is used. This method has certain robustness and reduces chattering compared with TOC at the cost of prolonging the response time [14], [15], which is not an optimal solution for high-quality servo systems requiring fast response.

Recently, another fast and smooth tracking method called the composite nonlinear feedback (CNF) control draws a lot of interest, which makes full use of both linear and nonlinear control techniques [16], [17], [18]. The linear feedback part is designed for quick response by manipulating the location of the conjugated pole pairs of the closed-loop system to have a small damping ratio. Meanwhile, the nonlinear part is built to increase the damping ratio of the closed-loop system as the output approaches the reference position to reduce the overshoot caused by the small damping ratio in the linear part [19]. This method has the potential of high-precision tracking. However, the performance of this conventional CNF is neither robust to disturbances nor the change of reference signal. Consequently, the controller parameters especially those for nonlinear feedback laws need retuning to maintain stability and the best transient performance every time the operating condition changes, which is painstaking and not applicable [20], [21]. Some techniques are introduced including the unified control scheme [22], enhanced CNF control with an additional integration action [23], and CNF with a Luenberger disturbance observer to solve this problem [24]. Unfortunately, these additional designs may be either conservative or not satisfactory and thus cause performance deficiency.

Hence, inspired by the track seeking and track following procedure in HDD control field [25], a novel two-phase MSC strategy containing a fast-response phase and a high-precision settling phase is proposed for PMSM servo systems which specially work on a point-to-point pattern with no load torque and a fixed inertia in this paper. Each phase of the MSC can be optimally designed to meet specific requirements such as minimum time approaching or minimum position error variance so that perfect fast response and high-precision PMSM tracking performance can be achieved.

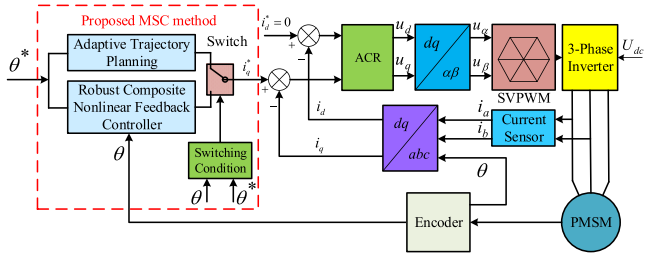

Fig. 1. Diagram of the proposed MSC method.

As for the fast-response phase, an adaptive trajectory planning (ATP) method for q-axis current is proposed based on Pontryagin's minimum principle [28] considering speed, acceleration, and jerk constraints to achieve time-optimal reaching ability over other control methods such as PI, PTOS, or PTOS based MSC in [20] and [27] while holding properties such as simple, effective and need less calculation at the same time. The idea that skipping the speed and position loop with the preplanned q-axis current trajectory is first attempted in this article considering that the current loop has the largest bandwidth in a servo system. Therefore, the response speed can be largely improved compared with the conventional three-loop PI cascaded control structure and the motor can reach the neighborhood of the reference position in minimum time. Also, compared with traditional TOC, the proposed method gets rid of the switching curve concept that may cause chattering while retaining the same time-optimal property in tracking process.

Afterward, similar to the track following stage, an extended state observer (ESO) based robust composite nonlinear feedback (RCNF) controller is designed for obtaining high-precision settling after the tracking error enters the neighborhood of zero, which is called high-precision settling phase. The system's lumped disturbances can be observed and compensated while the position response hardly has any overshoot. Also note that when the mode switching happens under the designed switching condition, the motor position always resides in the neighborhood of the reference signal, which means that the equivalent reference signal for this RCNF controller is a small value around zero whatever the position reference is. Hence, RCNF parameter readjustment is hardly required once the parameters are fixed in the tuning process and the system is robust enough to disturbances as well as the change of reference position by our design. The overall diagram of the proposed MSC method is depicted in Fig. 1 where the value with asterisk means the reference value.

The main contributions of this article are listed as follows.

1) An effective MSC control scheme is put forward for point-to-point PMSM servo systems and a novel q-axis current trajectory planning method for fast-response phase is designed. This trajectory planning method can achieve time-optimal tracking without chattering compared with conventional TOC. The idea that skipping speed and position loop with preplanned q-axis current trajectory is first attempted in a PMSM servo system.
2) The external disturbances in the kinematical equation is discussed and modeled in detail for the target

application scenario. An intuitive adaptive trajectory planning (ATP) method based on the least square method (LSM) acceleration estimation and area equivalence principle is developed to add robustness to the whole system.

3) In the high-precision settling phase, a novel RCNF controller is designed with an external ESO disturbance observer. Satisfactorily precise tracking is ensured and it is proved that this RCNF controller is robust enough to disturbances as well as the change of reference position in the proposed MSC structure.

The structure of this article is arranged as follows. Section II illustrates the proposed ATP method for fast-response phase. The basic principle and formulas of the time-optimal trajectory planning method are discussed first. And the disturbance in PMSM kinematical equation is modeled with the proposed adaptive law introduced to improve robustness. Section III contains the RCNF controller for high-precision settling phase where a full-order ESO for disturbance and speed estimation is constructed. The RCNF design procedure is then presented with stability mathematically proved. Finally, in Section IV, experimental results prove the effectiveness and robustness of the proposed MSC method.

II. Time-Optimal Adaptive Current Trajectory Planning for Fast-Response Phase

In this section, the PMSM mathematical model and position tracking servo problem are formulated. Then, a time-optimal q-axis current trajectory is planned based on the trajectory planning theory for the fast response phase. An adaptation law is further introduced to add robustness to this method and the implementation steps of ATP is briefly summarized.

A. Problem Formulation

The mechanical expression of PMSM servo system can be considered as a double-integrator model depicted by the state equation (1) with the overall lumped disturbance included

$$\begin{cases} \dot{x} = Ax + B(u+d) \\ y = Cx \end{cases} \tag{1}$$

with

$$x = \begin{pmatrix} x_1 \\ x_2 \end{pmatrix} = \begin{pmatrix} \theta \\ \omega \end{pmatrix}, A = \begin{pmatrix} 0 & 1 \\ 0 & 0 \end{pmatrix}, B = \begin{pmatrix} 0 \\ b \end{pmatrix}, C = \begin{pmatrix} 1 \\ 0 \end{pmatrix}^T$$

where the rotor position θ can be acquired by the encoder; $b = K_t/J$ is the acceleration constant; the control law u means the q-axis current in a PMSM servo system which is normally clamped by a saturation function "sat(u)." Also, the lumped disturbances d can be assumed as a constant or slowly varying further illustrated in the following section.

The PMSM servo problem can be depicted as (2) in which a proper control signal u is designed to navigate the motor starting from a negative position (by proper coordination transformation) to the origin of the (θ, ω) phase plane in consideration of different purposes, such as time-optimality or minimum energy [29]

$$\begin{cases} \theta(0) = -r_0; \theta(t_f) = 0; r_0 > 0 \\ \omega(0) = 0; \omega(t_f) = 0; |u| \le i_{\max}; |\omega| \le \omega_{\max}. \end{cases} \tag{2}$$

B. Time-Optimal Current Trajectory Planning

In this part, a time-optimal seven segment q-axis current trajectory planning method is proposed for the fast-response phase. The shape of this current profile is deduced based on the TOC theory first. Furthermore, different cases are considered and mathematical calculation is shown in detail for implementation.

Since an ideal PMSM servo system should track the reference signal both fast and accurately, time-optimality is the primary objective in the fast-response phase. A time-optimal q-axis current trajectory that guarantees least tracking time is preferred in the fast-response phase. According to the optimal control theory [28], the condition for this second-order system to reach the reference position in minimum time is that first a positive maximum input signal $u_{\max}$ ($i_{\max}$) is exerted followed by the negative maximum control $-u_{\max}$ ($-i_{\max}$) after the switching instant, which can be regarded as a bang-bang behavior. The control has only one switching for second-order systems according to Pontryagin's minimum principle if the disturbance in (1) is ignored. Typically, the switching condition from the maximum to minimum control is depicted by a so-called switching curve in phase plane as (3) and switching happens when the system states go across the curve. If the initial state locates on these two lines, no switching is required

$$\begin{cases} \delta_- = \{(\theta, \omega) | \theta = -\omega^2/2u_{\max}\} \\ \delta_+ = \{(\theta, \omega) | \theta = \omega^2/2u_{\max}\}. \end{cases} \tag{3}$$

However, the conventional TOC exhibits unacceptable chattering since the system states cannot stay identically on the switching curve because of measurement error and disturbance. Hence, a novel trajectory planning method without the concept of switching curve is proposed which inherits the time-optimal nature of TOC and avoids chattering. Here, a time-optimal q-axis current trajectory imitating TOC bang-bang control profile is preplanned online based on the given reference position along with the motor model. And this control directly serves as the current controller reference, which skips both speed and position controllers to make full use of the servo system's bandwidth. Normally, the dynamics of current tracking can be ignored [31], which means that the motor's q-axis current can track the reference trajectory seamlessly. In this case, time-optimal tracking can be guaranteed without any chattering. The detailed procedure is illustrated in the remaining part of this section.

Assume that the position reference is larger than the initial motor position. Based on the analysis above, three phases can be identified generally in a complete servo process: acceleration phase where the motor accelerates at the maximum acceleration $a_{\max}$, maximum velocity phase in which the motor operates at maximum angular velocity $\omega_{\max}$ and deceleration phase whose profile is opposite to the acceleration phase. According to the magnitude of the reference, two different profile shapes can be distinguished when designing the q-axis current where the difference lies in that whether there is a maximum velocity

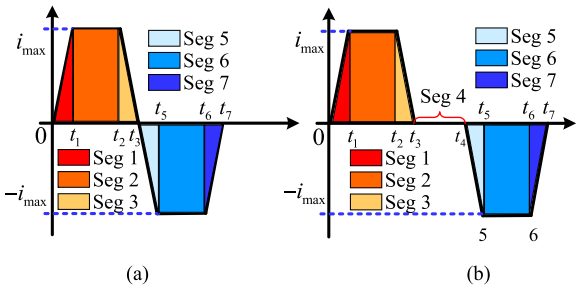

Fig. 2. Smoothened q-axis current trajectory profile under different scenarios. (a) Position reference smaller than critical value S_{c2}. (b) Position reference bigger than critical value S_{c2}.

phase. It is also noteworthy that a discontinuous acceleration may generate efforts and stresses on the PMSM mechanical system resulting in detrimental or generating undesired vibrational phenomena [30]. Therefore, the aforementioned profile can be smoothened by the introduction of jerk (the time derivative of acceleration). Accordingly, the two different preplanned q-axis current trajectories with time-optimality is shown as Fig. 2, where a linear transition with the slope of the maximum jerk $j_{\max}$ or the minimum value $-j_{\max}$ is inserted between the maximum acceleration and zero. Each trajectory contains seven segments along with seven switching instants in the general situation, where the situation in (a) is called a triangular case and (b) is the trapezoidal case. Here the task converts to design the seven switching instants t_1 to t_7 based on the reference position and the motor kinematical model.

The critical reference position S_{c2} that distinguishes these two profile shapes should be acquired before the trajectory is planned and the formula is displayed as follows:

$$S_{c2} = 2(\Delta_1 + \Delta_2 + \Delta_3) = a_{\max}\omega_{\max}/j_{\max} + \omega_{\max}^2/a_{\max} \tag{4}$$

where Δ_1, Δ_2, and Δ_3 are the area (motor displacement) covered by the colored segments Seg1, 2, and 3 in Fig. 2, respectively; $a_{\max} = K_t i_{\max}/J$ is the maximum acceleration, while $\omega_{\max}$ and $j_{\max}$ are predefined values considering the PMSM mechanical system.

Therefore, the following cases distinguished by the position reference are discussed in our proposed trajectory planning method. And further calculations are performed to ensure that the preplanned current trajectory will perfectly drive the motor to track the reference position.

1) Case I: If the position reference is too tiny and smaller than the critical value $S_{c1} = 2a_{\max}^3/j_{\max}^2$, that is, even the maximum acceleration is not reached, the system directly switches to RCNF controller in the settling phase illustrated in the next section. The reason is that initially the motor position is close enough to the reference and high accuracy is the most concern in this case. Note that typically S_{c1} is really small and this case is fairly uncommon.
2) Case II: On this scenario, the motor does not have a constant velocity phase. The current profile takes the form of Fig. 2(b) when the position reference satisfies $S_{c1} < r_0 \le S_{c2}$, which means that the maximum velocity is not reached in the whole servo process. From 0 to t_1, the q-axis current increases at the slope of maximum jerk $j_{\max}$ before the current arrives at its maximum value and from t_1 to t_2, the current holds its maximum value. After that, it decreases linearly at $-j_{\max}$ from t_2 to t_5 until $-i_{\max}$ is reached with t_3 equals to t_4. Finally, the q-axis current holds the value $-i_{\max}$ from t_5 to t_6 and diminishes to 0 during t_6 to t_7. Clearly, the corresponding PMSM angular velocity has a quasi-triangular profile and each switching instant t_1 to t_7 can be acquired by (5) through model-based calculation

$$\begin{cases} t_1 = a_{\max}/j_{\max}; t_2 = t_3 - a_{\max}/j_{\max} \\ t_3 = a_{\max}/2j_{\max} + \sqrt{(a_{\max}/2j_{\max})^2 + r_0/a_{\max}} \\ t_4 = t_3; t_5 = t_4 + a_{\max}/j_{\max} \\ t_6 = 2t_4 - a_{\max}/j_{\max}; t_7 = 2t_3. \end{cases} \tag{5}$$

3) Case III: In this case, condition $r_0 > S_{c2}$ holds [see Fig. 2(b)]. Different from case II, the motor has a constant speed duration after the angular velocity reaches its limitation. Hence, the speed controller, for example, a PI controller, is plugged in between t_3 and t_4 in Seg4 in Fig. 2(b) to maintain the maximum speed. Except for that, the rest part of the trajectory is exactly the same as case II and the formula for each switching instants can be calculated as follows:

$$\begin{cases} t_1 = a_{\max}/j_{\max}; t_2 = \omega_{\max}/a_{\max} \\ t_3 = a_{\max}/j_{\max} + \omega_{\max}/a_{\max} \\ t_4 = t_3 + (r_0 - S_{c2})/\omega_{\max} \\ t_5 = t_4 + t_1; t_6 = t_4 + t_2; t_7 = t_4 + t_3. \end{cases} \tag{6}$$

Since the proposed time-optimal q-axis current profile has been programmed mathematically, this trajectory is then treated as the reference of the q-axis current controller in the fast-response stage, which can navigate the motor to the neighborhood of the desired position in minimum time and make the system have the largest bandwidth. When a new position reference is given, the corresponding current trajectory is planned online in microprocessors and then get implemented to the motor. After this stage, a switching condition is designed and the system switches to the high-precision settling phase to completely eliminate the tracking error.

C. Disturbance Modeling of PMSM

Unfortunately, in reality, the motor suffers from various disturbances both internally and externally and the influence of the d term in (1) cannot be neglected. Hence, the performance of the proposed trajectory planning method will be largely deteriorated and greatly prolongs the settling time or even cause system failure. With this in mind, an adaptation law is of necessity to endow robustness to this fast-response trajectory planning method. This part gives a deep insight on the various sources of disturbance in PMSM and fortunately the disturbance d can be assumed as a constant or slowing varying in our target working

scenario by the following reasoning:

$$|(y - r_0)/r_0| < \gamma. \tag{7}$$

From [32], the kinematic equation of the PMSM in (1) can be further expressed as (8) considering the overall disturbances in the real application

$$\frac{d\omega}{dt} = \frac{3p\psi_{f0}i_q}{2J} + \frac{3p\Delta\psi_f i_q}{2J} - \frac{T_L}{J} - \frac{T_f}{J} - \frac{T_{cog}}{J} - \frac{B\omega}{J} \tag{8}$$

where $\Delta\psi_f = \psi_f - \psi_{f0}$ is the flux mismatch between the real value ψ_f and the nominal one ψ_{f0}.

According to the analysis above, the trajectory planning method aims at the point-to-point servo working pattern with no load torque and a fixed inertia. Hence, the unexpected load torque T_L can be assumed to be zero. Among the other disturbances, the viscous damping coefficient B is a tiny value and thus the $B\omega$ term is negligible [33]. Friction torque T_f can be modeled by the Coulomb friction model [34] and can be assumed as a constant if the motor rotates in one direction. As for the term containing flux linkage mismatch $\Delta\psi_f$, it can also be treated as unchanged when the q-axis current is a constant, which takes up most of the servo process.

Also, the cogging torque can be modeled as follows [35]:

$$T_{\text{cog}} = \sum_{i=1}^{\infty} T_{\text{cog}i} \cos(iQ\theta + \varphi_i)$$

where T_{cogi} and φ_i are the corresponding amplitude and phase angle of different order cogging torque harmonics. This term can also be neglected for two reasons. On one hand, the amplitude of the cogging torque is fairly small relative to the electromagnetic torque. On the other hand, it is reasonable to assume that the average effect of the sinusoidal shape T_{cog} to be zero during one servo operation.

From the analysis above, the combined impact of all these disturbances can be treated as a constant or slowly varying value in a whole servo process. Consequently, it is reasonable to rewrite (8) in the form of (9) where the time derivative of d is zero. Hence, the adaptive law can be designed based on the difference between the nominal acceleration and the real one caused by the disturbance term d

$$\begin{cases} \frac{d\omega}{dt} = \frac{3p\psi_{f0}}{2J}(i_q + d) \\ \dot{d} = 0 \end{cases}. \tag{9}$$

D. Proposed Adaptive Law Design

According to the analysis above, the constant acceleration mismatch caused by the slowly varying disturbance d will slow down the acceleration process and if the real acceleration is different from the nominal one $a_{\max}$, the preplanned q-axis current trajectory cannot drive the motor to the close neighborhood of the desired destination. Hence, an effective adaptive law which consists of the acceleration estimation and trajectory modification is designed to add robustness to the proposed trajectory planning method.

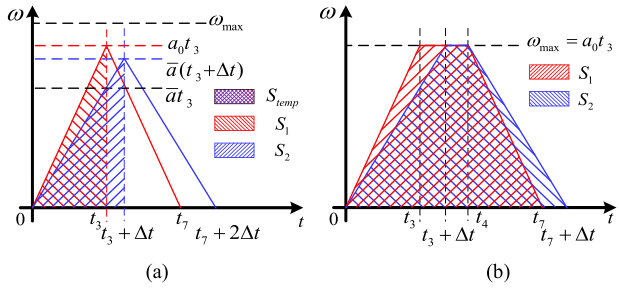

Fig. 3. Nominal speed profile (red) and the profile after q-axis current adaptation (blue). (a) Triangular case. (b) Trapezoidal case.

First, the real acceleration of the motor should be estimated. In such applications where the servo system works on a point-to-point pattern with no load torque and a fixed inertia, the speed is in proportional to time under constant acceleration ($i_{\max}$) with equation $\omega = \bar{a}t$ holds and a least square method (LSM) is designed to extract the real acceleration $\bar{a}$. According to the preplanned current profile, the motor should accelerate at the maximum constant acceleration driven by the maximum q-axis current $i_{\max}$ from t_1 to t_2. During this period, a series of time versus angular velocity data pairs are collected evenly from t_1 to $(t_2 + t_1)/2$ by microprocessors. The distribution of these points has the shape of $\omega = \bar{a}t$ where the velocity grows proportionally with time. Hence, the real motor acceleration $\bar{a}$ can be estimated by LSM as (10) which can be regarded as accurate and unbiased [37]

$$\bar{a} = \frac{\sum \omega_i t_i - \sum \omega_i \sum t_i}{\sum t_i^2 - (\sum t_i)^2} \tag{10}$$

where t_i means the sampling moments and ω_i represents the corresponding motor angular velocity.

Then, this estimated $\bar{a}$ is used as a feedback term to correct the preplanned current profile. It is known that the area enclosed by the axis and speed curve denotes the position value. From Fig. 2, the corresponding speed trajectory for two different cases can be approximated as a symmetrical triangle or trapezoid respectively as the red lines in Fig. 3 where the shadow means the angle that the motor rotates driven by the preplanned current profile. Considering about disturbances, each one of t_2 to t_7 should be adapted based on $\bar{a}$ to form a new trajectory as the blue lines in Fig. 3 so that even if the nominal acceleration $a_{\max}$ is perturbed by disturbances, the modified current trajectory can still force the motor to reach the desired position as before. Therefore, the adaptive law is built based on the "area equivalence principle" where the preplanned trajectory is modified to make the area covered by both lines (S_1 for red and S_2 for blue) equal. Resultantly, the adaptive law has two forms corresponding to the two current profiles in Fig. 2 and the law is discussed as follows.

As for case II with no constant speed phase, the speed profile under the preplanned q-axis current trajectory can be simplified as a triangle in Fig. 3(a). For this case, the position covered by the red and blue lines should be equal as (11). And further the duration Δt that needs to be compensated on the switching instants can be expressed as (12) where a_0 represents the nominal acceleration ($a_{\max}$) used for trajectory planning. Each modified

TABLE I
DIFFERENT ADAPTIVE CASES WITH SWITCHING TIME MODIFICATION

	t_1'	t_2'	t_3'	t_4'	t_5'	t_6'	t_7'
$r_0 \le S_{c2}$	t_1	$t_2+\Delta t$	$t_3+\Delta t$	$t_4+\Delta t$	$t_5+\Delta t$	$t_6+2\Delta t$	$t_7+2\Delta t$
$r_0 > S_{c2}$	t_1	$t_2+\Delta t$	$t_3+\Delta t$	t_4	t_5	$t_6+\Delta t$	$t_7+\Delta t$

switching moment is shown in the first row in Table I

$$\frac{S_2}{S_1} = \frac{S_2}{S_{\text{temp}}}\frac{S_{\text{temp}}}{S_1} = \frac{a_0}{\bar{a}}\left(\frac{t_3}{t_3+\Delta t}\right)^2 = 1 \tag{11}$$

$$\Delta t = \left(\sqrt{a_0/\bar{a}} - 1\right) t_3. \tag{12}$$

As for case III with constant maximum speed case in Fig. 3(b), the trapezoidal speed trajectory is initially planned. The switching time compensation term Δt is deducted as (13). Accordingly, all the other modified switching instants are shown in the lower row in Table I

$$\Delta t = (a_0 - \bar{a})t_3/\bar{a}. \tag{13}$$

After adaptation, the modified trajectory is shaped by the new switching instants from t'_2 to t'_7 and then implemented to the motor. Navigated by the new current profile, the motor can move toward the reference position as close as possible.

Another point to say is that the definition of "enough speed versus time data pairs" in acceleration estimation is introduced. In fact, we find out that a minimum of ten points is fairly sufficient and can guarantee an accurate acceleration estimation in this one-dimension linear regression problem by trial and error. If the position reference is too small to sample ten valid points in the acceleration phase, there is no need to use the adaptive law because the high-precision settling stage itself can stabilize the system fast and precisely under such a tiny position command, not to mention the trajectory planning method is implemented in the first stage.

To conclude, the analysis above covers all possible current trajectory planning adaptation situations and by this adaptive law, the proposed ATP method has robustness to disturbances.

E. Switching Condition Design

By the analysis above, the servo motor will follow the time-optimal current trajectory initially and then the settling phase takes over. Considering this, the whole q-axis current trajectory is not fully exerted because when the proximity of reference position is approached, time-optimality is not the top priority while the high-accuracy settling is. Therefore, the switching condition can be designed as (7), which means that the controller switches to RCNF for high-precision settling once the motor position reaches the small neighborhood of the reference.

A proper γ is chosen to depict the range of the switching neighborhood. Typically for a high-precision servo system, 2% error band system settling time ($\gamma = 0.02$) is adopted as a tradeoff between fastness and precision [36].

Another case may happen if the system is affected by severe disturbance where the switching condition (7) will not be satisfied despite adaptation is used in the ATP process. In this case, the switching happens after the current trajectory is fully exerted. To conclude, the switching condition is triggered when the motor position reaches 2% error band or the whole current trajectory is completely exerted.

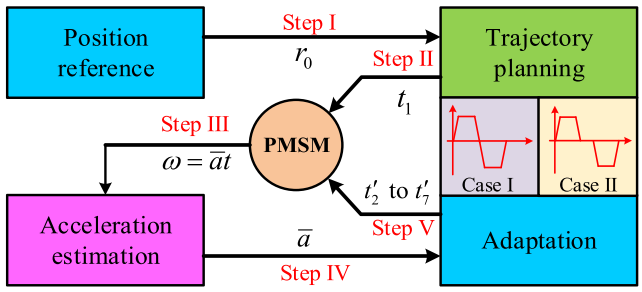

Fig. 4. Implementation procedure of the proposed ATP method.

F. Implementation Procedure of ATP

The detailed implementation steps of the proposed ATP are discussed in this part and the procedure is also depicted by the flowchart in Fig. 4.

1) Trajectory Planning: In the first step, the shape of the q-axis current trajectory is determined based on the critical position and reference position. And the original seven segment q-axis current trajectory is preplanned by the nominal motor model according to Section II-B.

2) Acceleration: The seven segment current profile shaped by t_1 to t_7 is then implemented to the q-axis current controller and the servo process starts. In this step, part of the original trajectory from 0 to somewhere before t_2 is used. In this period, the motor accelerates at a constant acceleration $a_{\max}$ driven by the maximum q-axis current $i_{\max}$ and afterward the modified trajectory takes over.

3) Acceleration Estimation: In this step, a series of time versus angular velocity data pairs, for example,, 20 pairs in our experiments are collected evenly from t_1 to $(t_2+t_1)/2$ by microprocessors. The distribution of these points has the shape of $\omega = \bar{a}t$ where the velocity grows proportionally with time. The least square method in (10) is then implemented on these data pairs and an unbiased real motor acceleration $\bar{a}$ is estimated before t_2.

4) Adaptation: Dependent on the position reference r_0, one of the adaptive laws in (12) or (13) is selected accordingly for adaptation and the compensation term Δt is acquired. The modified switching moments t'_2 to t'_7 are then calculated as Table I which forms the modified current trajectory.

5) Modified Trajectory Implementation: After adaptation, the modified trajectory can be acquired based on t'_2 to t'_7 and then implemented to the motor. Note that the second switching moment here is t'_2 instead of t_2. Navigated by the new trajectory shaped by t'_2 to t'_7, the motor can move toward the reference position as close as possible. Thus, the system gains satisfying robustness to disturbances by the ATP design.

In summary, the ATP method can be regarded as a two-stage trajectory planning method, where the first stage is built for

time-optimal tracking and the other one for robustness issue. The main purpose of ATP is to ensure the motor to reach the near neighborhood of the desired position despite of external disturbances. After the switching happens, the controller will switch to RCNF for unbiased tracking that is discussed in detail in Section III.

III. Robust Composite Nonlinear Feedback Controller Design for the Settling Phase

In this section, an RCNF controller is built for the high-precision settling after the controller switching happens. First, a full-order ESO is designed for speed and disturbance observation. Based on this observer, the RCNF control law for PMSM is illustrated and the whole MSC method convergence is strictly proved.

A. Extended State Observer Design

From the analysis above, it is necessary to build an external observer to obtain the rotor speed signal based on the position message from the encoder for position control. Moreover, the overall disturbances need to be considered when a controller is constructed to eliminate the steady-state tracking error and achieve high quality settling. Considering the PMSM kinematical equation with disturbance as (9), a third-order ESO can be designed as follows:

$$\begin{cases} \dot{z}_1 = z_2 + L_1(z_1 - \theta) \\ \dot{z}_2 = z_3 + bi_q + L_2(z_1 - \theta) \\ \dot{z}_3 = L_3(z_1 - \theta). \end{cases} \tag{14}$$

The observer is a third-order type with z_1, z_2, and z_3 estimating θ, ω, and d, respectively. Meanwhile, the ESO gains can be designed as $L_1 = -3\omega_c, L_2 = -3\omega_c^2$, and $L_3 = -\omega_c^3$, where ω_c is the only tunable coefficient determining the ESO bandwidth. The observed state z_2 and z_3 will be used in the proposed RCNF controller afterward.

Define the observation error
$e = (\, e_1 \; e_2 \; e_3 \,)^T = (\, z_1 \; z_2 \; z_3 \,)^T - (\, \theta \; \omega \; d \,)^T$.
Clearly, the error equation can be written as follows:

$$\dot{e} = A_e e \tag{15}$$

where

$$A_e = \begin{pmatrix} L_1 & 1 & 0 \\ L_2 & 0 & 1 \\ L_3 & 0 & 0 \end{pmatrix}.$$

According to the Lyapunov stability theory [12], there always exists a unique solution $Q > 0$ for Lyapunov equation (16) given a positive-definite matrix W_Q if A_e is stable

$$A_e^T Q + Q A_e = -W_Q. \tag{16}$$

B. RCNF Control Law Design

Similar to the design procedure in [19], a composite controller including a linear part and a nonlinear part is constructed. This controller serves as the main control law to eliminate tracking error fast and sound in the high-precision settling phase.

First, the linear feedback control law can be designed as follows:

$$u_l = F(x - x_e) \tag{17}$$

where $x_e = (r_0 0)^T$, $F = -[\omega_1^2/b \; 2\xi_1\omega_1/b] = [\, f_1 \; f_2 \,]$ is the feedback gain in which ω_1 means the natural frequency and ξ_1 denotes the damping ratio within (0,1). The gain is carefully designed to manipulate the closed-loop system's conjugated poles $\lambda_{1,2} = -\xi_1\omega_1 \pm j\omega_1\sqrt{1-\xi_1^2}$ to a proper position so that the best performance is ensured. Typically, the damping ratio ξ_1 should be small enough for the system to have a fast response when the tracking error is large, and the natural frequency ω_1 should be tuned a bit larger for a desired servo system bandwidth. Note that a too large ω_1 will bring in oscillation in the response. Therefore, a tradeoff between high bandwidth and oscillation need to be considered when tuning.

Obviously, a positive-definite matrix W_P can be selected as (18) and the corresponding Lyapunov equation (19) can be uniquely solved by P in the shape of (20)

$$W_P = \begin{pmatrix} 2\omega_1^4/b^2 & 0 \\ 0 & 2\omega_1^2\eta/b^2 \end{pmatrix}, \eta \in (0,1) \tag{18}$$

$$(A + BF)^T P + P(A + BF) = -W_P \tag{19}$$

$$P = \begin{pmatrix} \frac{\omega_1^2}{b^2} & \frac{\omega_1(1+\eta)}{2\xi_1 b^2} \\ \frac{\omega_1(1+\eta)}{2\xi_1 b^2} & \frac{2\xi_1\omega_1^3}{b^2} + \frac{\omega_1^3(1+\eta)}{2\xi_1 b^2} \end{pmatrix}. \tag{20}$$

In addition to the linear controller, the nonlinear feedback part of the composite controller is designed as follows:

$$u_n = \rho(e(t))F_n(x - x_e) = \rho(e(t))B^T P(x - x_e) \tag{21}$$

where $\rho(e(t))$ is a smooth nonlinear nonpositive function of the tracking error and will be discussed in detail later; the symbol F_n is defined as follows:

$$F_n = B^T P = \left[\frac{\omega_1(1+\eta)}{2\xi_1 b} \;\; \frac{2\xi_1\omega_1^3}{b} + \frac{\omega_1^3(1+\eta)}{2\xi_1 b} \right] := (f_{n1} f_{n2}).$$

The purpose of introducing the nonlinear control u_n is to increase the damping ratio of the closed-loop system as the motor position approaches the target reference to reduce the overshoot caused by the small damping ratio ξ_1 in the linear control. From the root locus theory, the closed-loop poles of the PMSM servo system will start from the open-loop poles of $F_n(sI - A - BF)^{-1}B$ as in [19], i.e., $\lambda_{1,2} = -\xi_1\omega_1 \pm j\omega_1\sqrt{1-\xi_1^2}$ in our design and end up at the open-loop zeros as $|\rho| \to \infty$, i.e., $z_1 = -\frac{2\omega_1\zeta_1}{1+\eta}$ and $z_2 = -\infty$. Obviously, the damping ratio grows when $|\rho| \to \infty$ and the system will have less overshoot. The location of the open-loop zero is highly dependent on η. And the tuning method of η is to choose an appropriate open-loop zero position so that the system will have satisfying damping ratio for a larger $|\rho|$, which corresponds to a smaller overshoot with a faster and more accurate response.

Considering that the speed and disturbance information have been already obtained from the ESO in (14), the final RCNF controller can be constructed as (22), which navigates the PMSM position to the set point value with fast convergence speed and

hardly any overshoot in the high-precision settling phase

$$u_{CNF} = u_l + u_n = (F + \rho F_n)\left(\begin{pmatrix} y \\ z_2 \end{pmatrix} - x_e\right) - z_3 \quad (22)$$

where $\tilde{x} = x - x_e = (\, y - r_0 \;\omega\,)^T$ and u_{CNF} means the RCNF controller output.

C. Overall Controller Stability Analysis

In this section, the convergence of the proposed MSC method is proved. Define $G_1 = (0\; f_2 - 1)$, $G_2 = (0\; f_{n2} 0)$ and we have the following theorem for MSC convergence.

Theorem 1: Considering the PMSM system in (1), the ATP method in Section II-F and the RCNF control law (22), the whole closed-loop system is stable and the motor can track the reference signal r_0 without any steady-state error if the following conditions are fulfilled.

1) There exists a positive scalar $\delta \in (0, 1)$ and a positive value c_δ such that for any scalar $\bar{x} = [\tilde{x} e]^T$ satisfying the following:

$$\forall \bar{x} \in \boldsymbol{X}\,(F, G_1, c_\delta) := \left\{ \bar{x} : \bar{x}^T \begin{bmatrix} P & 0 \\ 0 & Q \end{bmatrix} \bar{x} \le c_\delta \right\} \quad (23)$$

such that he following equation holds:

$$\left| \begin{bmatrix} F & G_1 \end{bmatrix} \bar{x} \right| \le (1 - \delta) u_{\max}. \quad (24)$$

On this scenario, $u_{\max}$ means the maximum allowed control signal which is the maximum allowed q-axis current in a PMSM system.

2) The level of the disturbance term d is bounded by the following:

$$|d| \le \delta u_{\max}. \quad (25)$$

3) When the controller switches to the settling phase, the system states (initial values) denoted by the subscription "0" $\bar{x}_0 = [\; y_0 - r_0 \;\omega_0 \;\; e_{10} \;\; e_{20} \;\; e_{30} \,]^T$ stays identically inside (23) as follows:

$$\bar{x}_0 \in \boldsymbol{X}\,(F, G_1, c_\delta)\,.$$

4) The nonpositive gain $\rho(e(t))$ is bounded by a certain value $\rho^* > 0$ such that expression $\rho^* > |\rho(e(t))|$ holds.

Proof: The working procedure of the proposed MSC method is that for any given position reference r_0, the ATP navigates the motor to the neighborhood of reference as close as possible and the RCNF control law takes over after switching to ensure a fast and precise servo process.

At the switching moment, the initial system states can be expressed as $\bar{x}_0 = [\; y_0 - r_0 \;\omega_0 \;\; e_{10} \;\; e_{20} \;\; e_{30} \,]^T$ and the real motor position stays somewhere near the set point. From assumption (3), the initial state vector $\bar{x}_0$ is enclosed by a large enough region $\boldsymbol{X}(F, G_1, c_\delta)$ when the control law switches to the RCNF control law. Hence, the following part will show that with the RCNF method after switching, the system will converge to the position reference with asymptotical stability property guaranteed.

After the switching happens, the RCNF control law (22) can be rewritten as follows:

$$\begin{aligned} u_{CNF} = u_l + u_n &= (F + \rho F_n)\left(\tilde{x} + \begin{pmatrix} 0 \\ e_2 \end{pmatrix}\right) - (d + e_3) \\ &= F\tilde{x} + (0 f_2 - 1)e + \rho(F_n\tilde{x} + (0 f_{n2} 0)e_2) - d \\ &= F\tilde{x} + G_1 e + \rho(F_n\tilde{x} + G_2 e_2) - d \end{aligned} \quad (26)$$

where the linear control and disturbance term satisfies the following:

$$F\tilde{x} + G_1 e - d \le |F\tilde{x} + G_1 e| + |d| \le u_{\max}. \quad (27)$$

From the equation above, the linear control u_l can be regarded as always unsaturated and the saturation phenomenon is caused by the nonlinear control action u_n, which can be further denoted by v as follows:

$$v = \mathrm{sat}(u_{\mathrm{CNF}}) - (F\tilde{x} + G_1 e) + d. \quad (28)$$

Considering the control saturation and following the same reasoning as in [19], under three different cases: $u_{\mathrm{CNF}} < -u_{\max}$, $|u_{\mathrm{CNF}}| \le |u_{\max}|$, and $u_{\mathrm{CNF}} > u_{\max}$, (28) can be further rewritten as follows:

$$\begin{cases} \rho(F_n\tilde{x} + G_2 e_2) < v < 0 \; u_{\mathrm{CNF}} < -u_{\max} \\ 0 < v < \rho(F_n\tilde{x} + G_2 e_2) \; u_{\mathrm{CNF}} > u_{\max} \\ v = \rho(F_n\tilde{x} + G_2 e) \;\; |u_{\mathrm{CNF}}| \le |u_{\max}|\,. \end{cases} \quad (29)$$

Hence, for all the possible situations, v can be expressed in the form of the following equation:

$$v = q\rho(F_n\tilde{x} + G_2 e) \quad (30)$$

where q is some value within (0,1] and $q = 1$ means the control u_{CNF} is not saturated.

By plugging in this, the system with the overall control u_{CNF} based on the analysis above can be expressed as follows:

$$\dot{x} = Ax + B(F\tilde{x} + G_1 e + v). \quad (31)$$

Moreover, the corresponding error equation for the closed-loop system is represented as follows:

$$\begin{aligned} \dot{\tilde{x}} &= A(\tilde{x} + x_e) + B(F\tilde{x} + G_1 e + v) \\ &= (A + BF + q\rho BF_n)\tilde{x} + (BG_1 + q\rho BG_2)e. \end{aligned} \quad (32)$$

To analyze the closed-loop stability provided that the system's initial condition $\bar{x}_0$, the target reference r_0, the nonpositive gain $\rho(e(t))$, and the disturbance d satisfy those conditions listed in the theorem, a positive-definite Lyapunov function is built as (33), which is globally positive except at the origin

$$V = \begin{pmatrix} \tilde{x} \\ e \end{pmatrix}^T \begin{pmatrix} P & 0 \\ 0 & Q \end{pmatrix} \begin{pmatrix} \tilde{x} \\ e \end{pmatrix} = \tilde{x}^T P\tilde{x} + e^T Q e. \quad (33)$$

Then, the time derivative of (33) can be calculated along with the system trajectory as follows:

$$\begin{aligned} \dot{V} &= \dot{\tilde{x}}^T P\tilde{x} + \tilde{x}^T P\dot{\tilde{x}} + \dot{e}^T Q e + e^T Q\dot{e} \\ &= \begin{pmatrix} \tilde{x} \\ e \end{pmatrix}^T \begin{pmatrix} -W_P + 2q\rho PB^T BP & P(BG_1 + q\rho BG_2) \\ (BG_1 + q\rho BG_2)^T P & -W_Q \end{pmatrix} \begin{pmatrix} \tilde{x} \\ e \end{pmatrix} \end{aligned}$$

$$\leq \begin{pmatrix} \tilde{x} \\ e \end{pmatrix}^T \begin{pmatrix} -W_P & P(BG_1 + q\rho BG_2) \\ (BG_1 + q\rho BG_2)^T P & -W_Q \end{pmatrix} \begin{pmatrix} \tilde{x} \\ e \end{pmatrix}. \quad (34)$$

From the partitioned matrix theory, the time derivative of V is negative if condition (35) holds. And if the positive-definite matrix W_Q in (16) is chosen as (36), it is clear that there exists a scalar $\rho^* > 0$ such that for any smooth nonpositive function bounded by $\rho^* > |\rho(e(t))|$, inequality $\dot{V} < 0$ holds globally except at the origin

$$W_Q - (G_1 + q\rho G_2)^T B^T P W_p^{-1} P B (G_1 + q\rho G_2) > 0 \quad (35)$$

$$W_Q > G_1^T B^T P W_p^{-1} P B G_1. \quad (36)$$

Therefore, with V reaching infinity when $\bar{x} = [\tilde{x}\ e]^T$ tends to be infinite, the closed-loop system is asymptotically stable to the origin and the theorem is proved. ■

Another important issue is the selection of the nonpositive function $\rho(e(t))$. Note that the role of this term is to increase the damping ratio as the tracking error decreases in the high-precision settling process. A feasible and effective choice is written as (37) according to [24]

$$\rho = -\beta \left| e^{-\alpha |r_0 - y|} - e^{-\alpha \gamma r_0} \right| \quad (37)$$

where α and β are positive tunable parameters.

Obviously, from the switching moment to the zero tracking error instant, the amplitude of (37) changes increasingly from 0 to $\beta|1 - e^{-\alpha\gamma r_0}|$ according to the switching condition (7), which means that the damping ratio of the system increases as the tracking error grows smaller so that the overshoot can be suppressed [20]. The positive parameters α, β are responsible for the decaying rate and amplitude of the nonpositive function, respectively. The general guideline of tuning α, β is to choose a pair to make the nonpositive function ρ have a relatively big amplitude and a satisfying decaying rate as the tracking error decreases to zero, which subsequently means the closed-loop dominant poles have a large damping ratio. Typically, a large enough β is chosen first to get appropriate damping while a proper α is then tuned to have a desirable decaying rate. Note that α cannot be tuned too small.

In conclusion, the proposed RCNF controller (22) for the high-precision settling phase of the MSC method is proved to be stable and can ensure fast and precise settling performance. Moreover, there are five parameters to be tuned $(\alpha, \beta, \eta, \xi_1, \omega_1)$ and once the values are set, no big modifications are needed.

IV. Experimental Results

To verify the effectiveness of this proposed ATP and RCNF based MSC method, experiments are performed on a digital servo PMSM system platform based on TMS320F28335 as shown in Fig. 5. The PMSM used in this experiment is a surface-mounted type with an external inertia pad and both electrical and mechanical parameters are displayed in Table II. What is more, the PWM frequency is set as 10 kHz, which is the same as the current loop frequency. The control frequency of the RCNF controller is 2 kHz. Also, a dead zone is added whose length

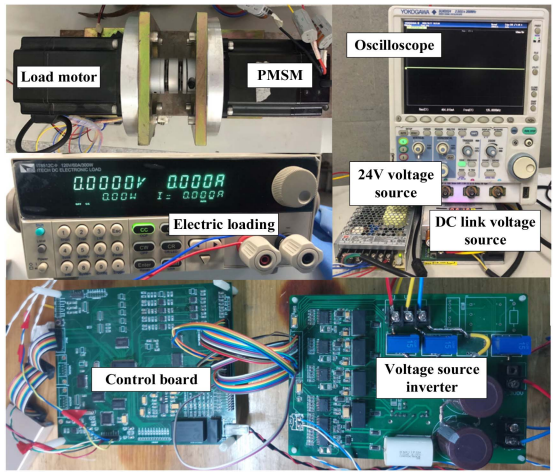

Fig. 5. Actual PMSM experimental platform.

TABLE II
Parameters Related to the Test Motor

Parameters	Value	Unit
DC-link voltage	120	V
Rated speed	1000	r/min
Pole pairs	5	
Flux linkage	0.059333	Wb
Inertia	0.00129	kg·m²

TABLE III
Performance Comparison of Settling Time (2%) in Milliseconds (ms)

Position reference (rad)		1	4	10
ATP with RCNF		52.2	100.6	171.6
PTOS		61.6	104.0	175.5
PI		67.2	104.6	172.5
Improvement compared with:	PTOS	9.4	3.4	3.9
	PI	15.0	4.0	0.9

is set as 1 μs. Note that to achieve seamless current tracking performance, the very popular predictive current control method with PI compensation is applied for the inner current loop as [10].

The maximum allowed q-axis current input is 3.6 A, i.e., $u_{\max} = 3.6$ A. By the motor parameters above, it can be calculated that $a_{\max} = 1241.8\,\mathrm{rad/s^2}$ and $j_{\max} = 6.2 \times 10^5\,\mathrm{rad/s^3}$. Meanwhile, $\gamma = 0.02$ is set for the switching condition and the maximum allowed angular velocity is set as 800 r/min. The experiments are carried out under three different position references from small to large to demonstrate the whole working scenario (namely, 1, 4, and 10 rad). Comparisons are also conducted with different control strategies (ATP with RCNF, PTOS, and PI) to prove the effectiveness and superiority of our proposed method. Note that there is no point of comparing with mere CNF method because the method is not robust to the reference change.

Since the settling time is the most concern in a PMSM servo system reflecting the tracking speed and overshoot, the detailed information when the motor enters 2% error band is zoomed in and summarized in Table III. Furthermore, to better illustrate the

TABLE IV
PERFORMANCE COMPARISON OF ENTRY TIME OF 0.01 RAD ERROR BAND IN MILLISECONDS (MS)

Position reference (rad)		1	4	10
ATP with RCNF		54.8	109.0	193.8
PTOS		64.4	113.2	197.4
PI		77.2	131.2	216.1
Improvement compared with:	PTOS	9.6	4.2	3.6
	PI	22.4	22.2	22.3

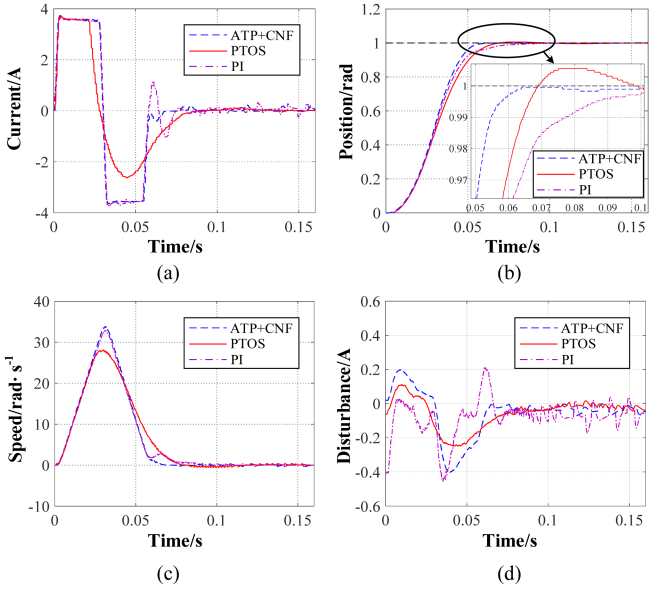

Fig. 6. Performance comparison under different control strategies (ATP with RCNF, PTOS, PI) with 1 rad reference position. (a) q-axis current. (b) Position reference and feedback. (c) Motor speed. (d) Estimated disturbance by ESO.

high-precision tracking property, Table IV lists the comparison of the time required for the PMSM to enter 0.01 rad error band. The controller parameterized by $(\alpha, \beta, \eta, \xi_1, \omega_1)$ is tuned as (5, 3.6, 0.25, 0.255, 54) for 1 and 4 rad case while for 10 rad case, the parameter pair are changed slightly to (5, 3.6, 0.32, 0.45, 54). This tiny change is reasonable because the position range of the 2% error band expands 10 times from 1 rad reference to 10 rad case. Moreover, the bandwidth ω_c for the external ESO is designed as 300 rad/s. In the experiment, the d-axis current reference is always set as zero. For comparison, the related PTOS parameters that determine the damping ratio, size of the linear region, and the discount factor are tuned for the best performance according to [14].

Figs. 6–8 show the experimental results when the position reference varies from 1 to 10 rad. And for comparison, both PI controllers for the speed loop and position loop are properly tuned to guarantee the best performance. In the 1 rad reference case in Fig. 6, it is obvious that the proposed ATP with RCNF method holds the best performance with the shortest settling time 52.2 ms and hardly any overshoot, indicating that this method is superior over the other two in fast tracking. When it comes to the entry time of 0.01 rad error band, the performance enhancement is impressive with 22.4 ms faster than conventional PI method and 9.6 ms quicker than PTOS, which proves that

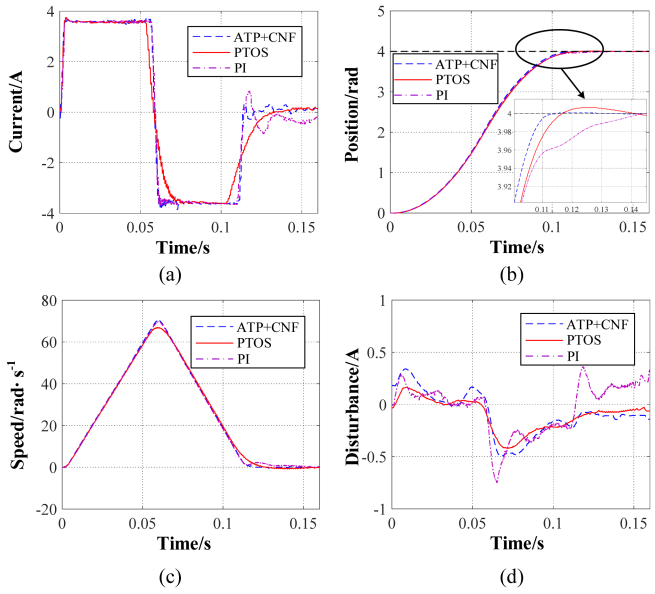

Fig. 7. Performance comparison under different control strategies (ATP with RCNF, PTOS, PI) with 4 rad reference position. (a) q-axis current. (b) Position reference and feedback. (c) Motor speed. (d) Estimated disturbance by ESO.

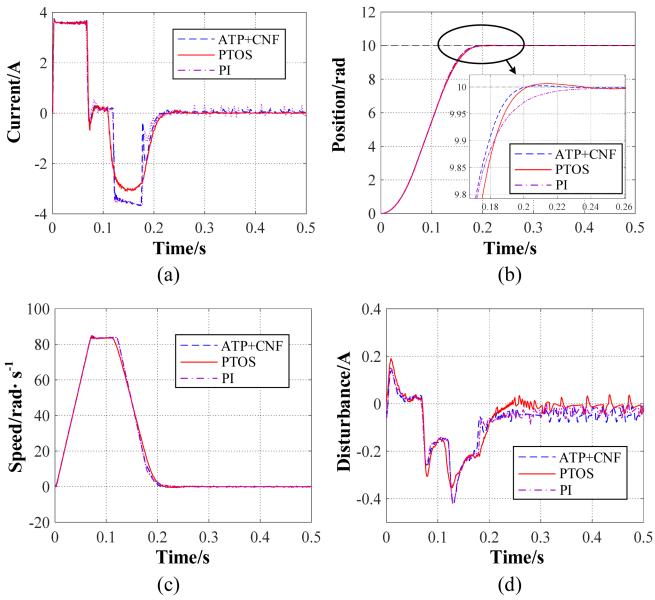

Fig. 8. Performance comparison under different control strategies (ATP with RCNF, PTOS, PI) with 10 rad reference position. (a) q-axis current. (b) Position reference and feedback. (c) Motor speed. (d) Estimated disturbance by ESO.

the proposed method also outperforms the other two methods in the high-precision tracking. As for the tracking results in Figs. 7 and 8 (4 and 10 rad, respectively), ATP with RCNF still performs much better compared with conventional PI method with about 20 ms earlier entering 0.01 rad error band. The settling time improvement is less noticeable compared with Fig. 6 since the large initial position gap drives the PI controller output to saturation easily. Moreover, even if PTOS boosts the servo performance of PI in some respects, the proposed ATP with RCNF controller shows significant superiority over PTOS

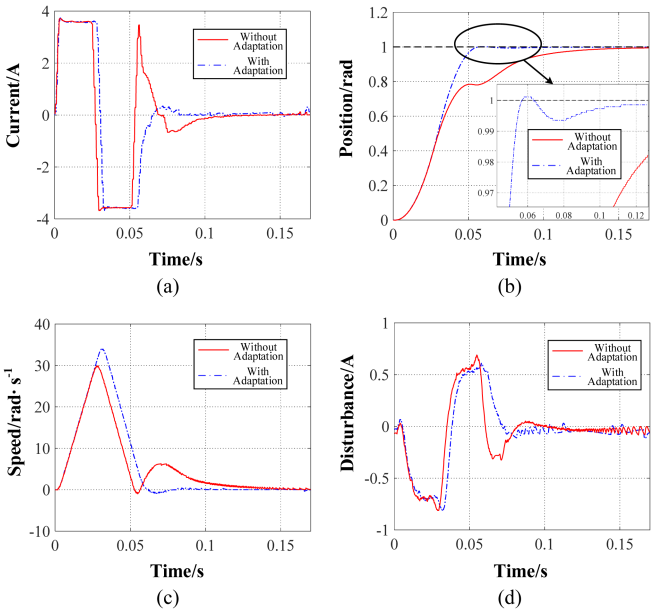

Fig. 9. Performance comparison with and without adaptive law in trajectory planning with 1 rad reference position and acceleration overestimated (20% larger than real). (a) q-axis current. (b) Position reference and feedback. (c) Motor speed. (d) Estimated disturbance by ESO.

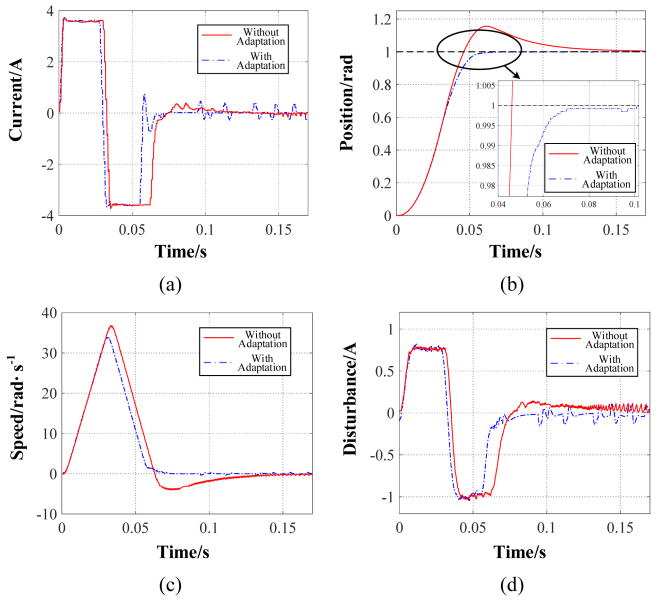

Fig. 10. Performance comparison with and without adaptive law in trajectory planning with 1 rad reference position and acceleration underestimated (20% smaller than real). (a) q-axis current. (b) Position reference and feedback. (c) Motor speed. (d) Estimated disturbance by ESO.

with about 4 ms both in settling time and in the entry time of 0.01 rad error band. Note that in Fig. 8(c), the constant velocity phase is constrained by a PI speed controller with $k_p = 0.1$ and $k_i = 0.01$ when the speed reaches its maximum allowed value.

From the results above, the proposed ATP with RCNF method holds the best performance both in fast-response and high-precision among the three methods. And the advantage over the most commonly used PI method is considerable. What is more, it is noticeable that PTOS does not exhibit expected fast tracking property even compared with PI. This is reasonable because PTOS is a conservative design of TOC and does not hold the time-optimal property. Hence, the unsaturated control in PTOS greatly slows down the tracking speed and prolongs the settling time. The proposed method makes up this shortcoming by the time-optimal property of ATP while the servo precision is further improved by RCNF.

Another group of experiments is conducted to testify the effectiveness of the proposed adaptive law under acceleration difference caused by the external disturbance term d such as large friction or unexpected load torque. Since it is really difficult to exert load or disturbance on the inertia pad while maintaining the original inertia, the external disturbance d is simulated by deviating the nominal acceleration a_0 deliberately from the real acceleration $\bar{a}$ driven by $u_{\max}$ when planning the current trajectory. In Fig. 9, a_0 is 20% larger than $\bar{a}$, which means that the equivalent overall disturbance amounts to 20% of the motor electromagnetic torque. As a result, the corresponding planned accelerating duration from t_1 to t_2 is much shorter than it should be. Hence, the motor cannot reach the tiny neighborhood of the desired location when the switching happens and the whole servo system responses really slow as the red line in (b). In contrast, with the adaptive law included, the settling time recovers to 51.8 ms, which is similar to the time-optimal performance in Fig. 6. The same principle applies to Fig. 10 where a_0 is 20% smaller than $\bar{a}$. The adaptive law also ensures the motor to track the reference with fast response and high precision. Clearly, the proposed adaptive law endows the proposed trajectory planning method with certain robustness against unexpected external disturbances.

Furthermore, the robustness of the proposed ATP and RCNF under inertia mismatch is proved. The nominal inertia is set as 50% and 200% of the real value, respectively, in our supplementary experiments at 1 rad position reference. In Fig. 11, the inertia used for trajectory planning is 0.00258 kg·m^2 (two times of the real value) and two different results with and without the adaptive law are compared. Clearly, without adaptation, the motor position has a huge overshoot to almost 2 rad before the RCNF law forces the position back to the reference. The response time increases significantly and this behavior can be called a servo system failure even if the system converges to the set point. In contrast, if the adaptive law is implemented as the blue line in the plot, the preplanned trajectory adjusts itself to an optimal one according to the real motor acceleration and the negative effect of the inertia mismatch is eliminated. And the servo process still holds the time-optimal property with a 51.5 ms settling time and 53.1 ms entry time to 0.01 rad error band. Similarly, the inertia used for trajectory planning is 0.000645 kg·m^2 (half the real value) in Fig. 12. With the proposed adaptation law, it can be seen that the motor behavior is good enough with a 51.4 ms settling time and 52.6 ms entry time to 0.01 rad error band, which has similar satisfactory performance to the one without inertia mismatch. Also note that ESO works well under inertia mismatch case because the model inaccuracy is included in the lumped disturbance. Another important fact to note is that the

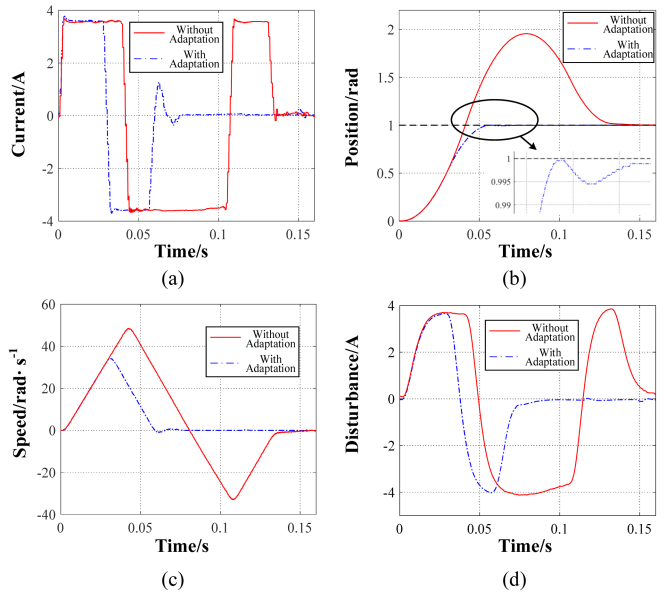

Fig. 11. Performance comparison with and without adaptive law in trajectory planning with 1rad reference position and nominal inertia two times of the real value. (a) q-axis current. (b) Position reference and feedback. (c) Motor speed. (d) Estimated disturbance by ESO.

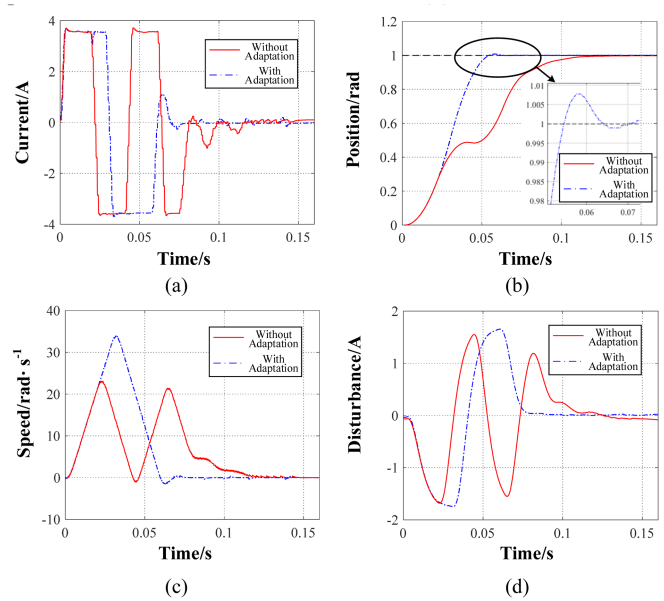

Fig. 12. Performance comparison with and without adaptive law in trajectory planning with 1 rad reference position and nominal inertia half the real value. (a) q-axis current. (b) Position reference and feedback. (c) Motor speed. (d) Estimated disturbance by ESO.

proposed MSC method has strong robustness to disturbances. From Figs. 11 and 12, the convergence property of our MSC still holds even if a failure happens in the fast-response phase, which proves the reasonableness of Condition (3) in Theorem 1.

Consequently, the proposed method is proved to have enough robustness to the inertia mismatch as well as external disturbance by experiments. It is also emphasized that even if the adaptive law endows the system with strong robustness, the mismatch between the nominal inertia and the real value should be as small as possible by certain advanced identification or measurement methods.

V. Conclusion

In this article, a novel MSC control scheme combining ATP and RCNF for PMSM servo systems to achieve fast response and high precision was put forward. Together with the adaptive law and ESO, the method is robust to various disturbances. Furthermore, the closed-loop stability was proved strictly and experiments were conducted on a real digital PMSM control platform. Results showed that in the fast-response phase, the ATP method performs much better than PI and PTOS especially when the position reference is not too large. Meanwhile in the high-precision settling phase, the RCNF appears impressive superiority. This proposed method is promising but a few challenges arise. For example, the optimized switching condition selection is an interesting topic and will be studied in the future.

References

[1] L. Wang, J. Su, and G. Xiang, "Robust motion control system design with scheduled disturbance observer," *IEEE Trans. Ind. Electron.*, vol. 63, no. 10, pp. 6519–6529, Oct. 2016.
[2] C. H. Liu and Y. X. Luo, "Overview of advanced control strategies for electric machines," *Chin. J. Elect. Eng.*, vol. 3, no. 2, pp. 53–61, Sep. 2017.
[3] L. Qi and H. Shi, "Adaptive position tracking control of permanent magnet synchronous motor based on RBF fast terminal sliding mode control," *Neurocomputing*, vol. 115, no. 4, pp. 23–30, Feb. 2013.
[4] Z. Ping, T. Wang, Y. Huang, H. Wang, J.-G. Lu, and Y. Li, "Internal model control of PMSM position servo system: Theory and experimental results," *IEEE Trans. Ind. Informat*, vol. 16, no. 4, pp. 2202–2211, Apr. 2020.
[5] H. Liu and S. Li, "Speed control for PMSM servo system using predictive functional control and extended state observer," *IEEE Trans. Ind. Electron.*, vol. 59, no. 2, pp. 1171–1183, Feb. 2012.
[6] S. Mandra, K. Galkowski, E. Rogers, A. Rauh, and H. Aschemann, "Performance-enhanced robust iterative learning control with experimental application to PMSM position tracking," *IEEE Trans. Control Syst. Technol.*, vol. 27, no. 4, pp. 1813–1819, Jul. 2019.
[7] F. Bu et al., "Rotor position tracking control for low speed operation of direct-drive PMSM servo system," *IEEE/ASME Trans. Mechatronics*, vol. 26, no. 2, pp. 1129–1139, Apr. 2021.
[8] M.-H. Park and C.-Y. Won, "Time optimal control for induction motor servo system," *IEEE Trans. Power Electron.*, vol. 6, no. 3, pp. 514–524, Jul. 1991.
[9] D. Verscheure, B. Demeulenaere, J. Swevers, J. D. Schutter, and M. Diehl, "Time-optimal path tracking for robots: A convex optimization approach," *IEEE Trans. Autom. Control*, vol. 54, no. 10, pp. 2318–2327, Oct. 2009.
[10] T. Türker, U. Buyukkeles, and A. F. Bakan, "A robust predictive current controller for PMSM drives," *IEEE Trans. Ind. Electron.*, vol. 63, no. 6, pp. 3906–3914, Jun. 2016.
[11] E. P. Ryan, "On the sensitivity of a time-optimal switching function," *IEEE Trans. Autom. Control*, vol. AC-25, no. 2, pp. 275–277, Apr. 1980.
[12] H. K. Khalil, *Nonlinear Systems*, 3rd ed. Upper Saddle River, NJ, USA: Prentice-Hall, 2002.
[13] M. L. Workman, R. L. Kosut, and G. F. Franklin, "Adaptive proximate time-optimal servomechanisms: Continuous time case," in *Proc. Amer. Control Conf.*, 1987, pp. 589–594.
[14] A. Dhanda and G. F. Franklin, "An improved 2-DOF proximate time optimal servomechanism," *IEEE Trans. Magn.*, vol. 45, no. 5, pp. 2151–2164, May 2009.
[15] A. T. Salton, Z. Chen, and M. Fu, "Improved control design methods for proximate time-optimal servomechanisms," *IEEE/ASME Trans. Mechatronics*, vol. 17, no. 6, pp. 1049–1058, Dec. 2012.
[16] C. Hu, R. Wang, F. Yan, and H. R. Karimi, "Robust composite nonlinear feedback path-following control for independently actuated autonomous vehicles with differential steering," *IEEE Trans. Transp. Electrific.*, vol. 2, no. 3, pp. 312–321, Sep. 2016.

[17] Y. Chen, C. Hu, and J. Wang, "Motion planning with velocity prediction and composite nonlinear feedback tracking control for lane-change strategy of autonomous vehicles," *IEEE Trans. Intell. Veh.*, vol. 5, no. 1, pp. 63–74, Mar. 2020.
[18] C. Hu, R. Wang, and F. Yan, "Integral sliding mode-based composite nonlinear feedback control for path following of four-wheel independently actuated autonomous vehicles," *IEEE Trans. Transp. Electrific.*, vol. 2, no. 2, pp. 221–230, Jun. 2016.
[19] B. M. Chen, T. H. Lee, K. Peng, and V. Venkataramanan, "Composite nonlinear feedback control for linear systems with input saturation: Theory and an application," *IEEE Trans. Autom. Control*, vol. 48, no. 3, pp. 427–439, Mar. 2003.
[20] G. Cheng and J. Hu, "An observer-based mode switching control scheme for improved position regulation in servomotors," *IEEE Trans. Control Syst. Technol.*, vol. 22, no. 5, pp. 1883–1891, Sep. 2014.
[21] W. Lan, C. K. Thum, and B. M. Chen, "A hard-disk-drive servo system design using composite nonlinear-feedback control with optimal nonlinear gain tuning methods," *IEEE Trans. Ind. Electron.*, vol. 57, no. 5, pp. 1735–1745, May 2010.
[22] C. K. Thum, C. Du, B. M. Chen, E. H. Ong, and K. P. Tan, "A unified control scheme for track seeking and following of a hard disk drive servo system," *IEEE Trans. Control Syst. Technol.*, vol. 18, no. 2, pp. 294–306, Mar. 2010.
[23] K. Peng, B. M. Chen, G. Cheng, and T. H. Lee, "Modeling and compensation of nonlinearities and friction in a micro hard disk drive servo system with nonlinear feedback control," *IEEE Trans. Control Syst. Technol.*, vol. 13, no. 5, pp. 708–721, Sep. 2005.
[24] G. Cheng and K. Peng, "Robust composite nonlinear feedback control with application to a servo positioning system," *IEEE Trans. Ind. Electron.*, vol. 54, no. 2, pp. 1132–1140, Apr. 2007.
[25] B. M. Chen, T. H. Lee, K. Peng, and V. Venkataramanan, *Hard Disk Drive Servo Systems*, 2nd ed. London, U.K.: Springer, 2006.
[26] T. Yamaguchi, H. Numasato, and H. Hirai, "A mode-switching control for motion control and its application to disk drives: Design of optimal mode-switching conditions," *IEEE/ASME Trans. Mechatronics*, vol. 3, no. 3, pp. 202–209, Sep. 1998.
[27] G. Cheng, K. Peng, B. M. Chen, and T. H. Lee, "Discrete-time mode switching control with application to a PMSM position servo system," *Mechatronics*, vol. 23, no. 8, pp. 708–716, Nov. 2013.
[28] F. L. Lewis, D. L. Vrabie, and V. L. Syrmos, *Optimal Control*, 3rd ed. Hoboken, NJ, USA: Wiley, 2012.
[29] Y. Wang, Y. Zhao, S. A. Bortoff, and K. Ueda, "A real-time energy-optimal trajectory generation method for a servomotor system," *IEEE Trans. Ind. Electron.*, vol. 62, no. 2, pp. 1175–1188, Feb. 2015.
[30] L. Biagiotti and C. Melchiorri, *Trajectory Planning for Automatic Machines and Robots*, 1st ed. Berlin, Germany: Springer, 2008.
[31] L. Rovere, A. Formentini, and P. Zanchetta, "FPGA implementation of a novel oversampling deadbeat controller for PMSM drives," *IEEE Trans. Ind. Electron.*, vol. 66, no. 5, pp. 3731–3741, May 2019.
[32] Y. Yan, J. Yang, Z. Sun, C. Zhang, S. Li, and H. Yu, "Robust speed regulation for PMSM servo system with multiple sources of disturbances via an augmented disturbance observer," *IEEE/ASME Trans. Mechatronics*, vol. 23, no. 2, pp. 769–780, Apr. 2018.
[33] S. Kim, "Moment of inertia and friction torque coefficient identification in a servo drive system," *IEEE Trans. Ind. Electron.*, vol. 66, no. 1, pp. 60–70, Jan. 2019.
[34] R. Garrido and A. Concha, "Inertia and friction estimation of a velocity-controlled servo using position measurements," *IEEE Trans. Ind. Electron.*, vol. 61, no. 9, pp. 4759–4770, Sep. 2014.
[35] N. Bianchi and S. Bolognani, "Design techniques for reducing the cogging torque in surface-mounted PM motors," *IEEE Trans. Ind. Appl.*, vol. 38, no. 5, pp. 1259–1265, Sep. 2002.
[36] J. Q. W. Duan, Q. N. He, Y. Mao, X. Zhou, and Q. T. Hu, "Proximate time-optimal servomechanism based on transition process for electro-optical set-point tracking servo system," *Appl. Sci.*, vol. 9, no. 23, Dec. 2019, Art. no. 5201.
[37] R. Isermann and M. Münchhof, *Identification of Dynamic Systems: An Introduction With Applications*, 1st ed. Berlin, Germany: Springer, 2011.

Shaobin Li was born in Liaoning, China, in 1997. He received the B.S. degree in electrical engineering from the Harbin Institute of Technology (HIT), Harbin, China, in 2019. He is currently working toward the Ph.D degree in the School of Electrical Engineering and Automation, HIT.

His current research interests include permanent magnet motor drives and control.

Yongxiang Xu (Member, IEEE) received the M.S. and Ph.D. degrees in electrical engineering from the Harbin Institute of Technology, Harbin, China, in 2001 and 2005, respectively.

In 2005, he joined the Department of Electrical Engineering, Harbin Institute of Technology, as an Assistant Professor. Since 2013, he has been a Professor with the Department of Electrical Engineering, Harbin Institute of Technology. His current research interests include permanent-magnet machine design and control.

Wentao Zhang was born in Shandong, China, in 1993. He received the B.S. degree in electrical engineering and automation from Harbin Institute of Technology, Weihai, China, in 2016, and the Ph.D. degree in electrical engineering from Harbin Institute of Technology, Harbin, China, in 2021.

He is currently a Lecturer with the Special Motor Research Center, Harbin Institute of Technology. His research interests include PMSM drives and control algorithms.

Jibin Zou (Senior Member, IEEE) received the M.S. and Ph.D. degrees in electrical engineering from the Harbin Institute of Technology, Harbin, China, in 1984 and 1988, respectively.

Since 1985, he has been engaged in the research in electrical machines. He was with the University of Liverpool, Liverpool, U.K., as a Visiting Research Fellow for one year. He is currently a Professor with the State Key Laboratory of Robotics and System, Harbin Institute of Technology. His current research interests include permanent-magnet machine design and control.

Dr. Zou has been a senior member of the IEEE Magnetics society, since 2000.